Anal. Chem. **2006,** *78,* 1061−1070

Counting Single Native Biomolecules and Intact Viruses with Color-Coded Nanoparticles

Amit Agrawal,[†] Chunyang Zhang,[†] Tyler Byassee,[†] Ralph A. Tripp,[‡] and Shuming Nie*,[†]

Departments of Biomedical Engineering and Chemistry, Emory University and Georgia Institute of Technology, 101 Woodruff Circle Suite 2001, Atlanta, Georgia 30322, and Centers for Disease Control and Prevention (CDC), and College of Veterinary Medicine, Department of Infectious Diseases, University of Georgia, Athens, Georgia 30602

Nanometer-sized particles such as semiconductor quantum dots and energy-transfer nanoparticles have novel optical properties such as tunable light emission, signal brightness, and multicolor excitation that are not available from traditional organic dyes and fluorescent proteins. Here we report the use of color-coded nanoparticles and dual-color fluorescence coincidence for real-time detection of single native biomolecules and viruses in a microfluidic channel. Using green and red nanoparticles to simultaneously recognize two binding sites on a single target, we demonstrate that individual molecules of genes, proteins, and intact viruses can be detected and identified in complex mixtures without target amplification or probe/target separation. Real-time coincidence analysis of single-photon events allows rapid detection of bound targets and efficient discrimination of excess unbound probes. Quantitative studies indicate that the counting results are remarkably precise when the total numbers of counted molecules are more than 10. The use of bioconjugated nanoparticle probes for single-molecule detection is expected to have important applications in ultrasensitive molecular diagnostics, bioterrorism agent detection, and real-time imaging and tracking of single-molecule processes inside living cells.

The detection and identification of single molecules represent the ultimate limit in chemical analysis, medical diagnostics, and in vivo molecular imaging.[1−4] By removing population averaging, single-molecule measurements can also provide new insights into the fundamental mechanisms of ligand−receptor binding, signal transduction, and intracellular transport. Recent advances have allowed direct imaging and dynamic studies of single biomacromolecules (e.g., DNA, RNA, and proteins)[5−7] as well as multicomponent molecular assemblies (e.g., molecular machines).[8−10] For applications in chemical analysis and medical diagnostics, however, single-molecule methodologies have achieved only limited success.[11−15] A major problem is that current organic dyes and fluorescent proteins are not bright or stable enough for routine single-molecule studies. Another problem is that target molecules often need to be chemically derivatized with a fluorophore, a difficult task for low-abundance genes and proteins. A further challenge is the need to discriminate bound targets from excess unbound probes in complex mixtures or inside living cells.

Here we report the use of bioconjugated nanoparticles and two-color fluorescence coincidence for real-time detection of single *native* biomolecules and intact viruses in a flow channel. Recent research by us and others has shown that nanometer-sized particles such as quantum dots (QDs) can be covalently linked with biorecognition molecules such as peptides, antibodies, or nucleic acids for use as fluorescent probes.[16−21] In comparison with organic dyes and fluorescent proteins, quantum dots and related nanoparticles exhibit unique optical and electronic properties such as size- and composition-tunable fluorescence emission, large absorption coefficients, and improved brightness and photostability.[22−24] By taking advantage of these properties, we

* To whom correspondence should be addressed. Tel: 404-712-8595, Fax: 404-727-9873, E-mail: snie@emory.edu.

† Emory University and Georgia Institute of Technology.

‡ CDC and University of Georgia.

(1) Nie, S.; Zare, R. N. *Annu. Rev. Biophys. Biomol. Struct.* **1997**, *26*, 567−596.
(2) Xie, X. S.; Trautman, J. K. *Annu. Rev. Phys. Chem.* **1998**, *49*, 441−480.
(3) Moerner, W. E.; Orrit, M. *Science* **1999**, *283*, 1670.
(4) Weiss, S. *Science* **1999**, *283*, 1676−1683.
(5) Ha, T. J.; Ting, A. Y.; Liang, J.; Caldwell, W. B.; Deniz, A. A.; Chemla, D. S.; Schultz, P. G.; Weiss, S. *Proc. Natl. Acad. Sci. U.S.A.* **1999**, *96*, 893−898.
(6) Ha, T. J. *Biochemistry* **2004**, *43*, 4055−4063.
(7) Zhuang, X. W.; Bartley, L. E.; Babcock, H. P.; Russell, R.; Ha, T. J.; Herschlag, D.; Chu, S. *Science* **2000**, *288*, 2048.
(8) Yildiz, A.; Forkey, J. N.; McKinney, S. A.; Ha, T. J.; Goldman, Y. E.; Selvin, P. R. *Science* **2003**, *300*, 2061−2065.
(9) Asbury, C. L.; Fehr, A. N.; Block, S. M. *Science* **2003**, *302*, 2130−2134.
(10) Wang, M. D.; Schnitzer, M. J.; Yin, H.; Landick, R.; Gelles, J.; Block, S. M. *Science* **1998**, *282*, 902−907.
(11) Castro, A.; Williams, J. G. *Anal. Chem.* **1997**, *69*, 3915−3920.
(12) Stoffel, C. L.; Rowlen, K. L. *Anal. Chem.* **2005**, *77*, 2243−2246.
(13) Li, H.; Zhou, D.; Browne, H.; Balasubramanian, S.; Klenerman, D. *Anal. Chem.* **2004**, *76*, 4446−4451.
(14) Li, H. T.; Ying, L. M.; Green, J. J.; Balasubramanian, S.; Klenerman, D. *Anal. Chem.* **2003**, *75*, 1664−1670.
(15) Foldes-Papp, Z.; Baumann, G.; Demel, U.; Tilz, G. P. *Curr. Pharm. Biotechnol.* **2004**, *5*, 163−172.
(16) Bruchez, M.; Moronne, M.; Gin, P.; Weiss, S.; Alivisatos, A. P. *Science* **1998**, *281*, 2013−2016.
(17) Chan, W. C. W.; Nie, S. M. *Science* **1998**, *281*, 2016−2018.
(18) Dubertret, B.; Skourides, P.; Norris, D. J.; Noireaux, V.; Brivanlou, A. H.; Libchaber, A. *Science* **2002**, *298*, 1759−1762.
(19) Jaiswal, J. K.; Mattoussi, H.; Mauro, J. M.; Simon, S. M. *Nat. Biotechnol.* **2003**, *21*, 47−51.
(20) Dahan, M.; Levi, S.; Luccardini, C.; Rostaing, P.; Riveau, B.; Triller, A. *Science* **2003**, *302*, 442−445.
(21) Lidke, D. S.; Nagy, P.; Heintzmann, R.; Arndt-Jovin, D. J.; Post, J. N.; Grecco, H. E.; Jares-Erijman, E. A.; Jovin, T. M. *Nat. Biotechnol.* **2004**, *22*, 198−203.
(22) Chan, W. C.; Maxwell, D. J.; Gao, X.; Bailey, R. E.; Han, M.; Nie, S. *Curr. Opin. Biotechnol.* **2002**, *13*, 40−46.
(23) Alivisatos, P. *Nat. Biotechnol.* **2004**, *22*, 47−52.

10.1021/ac051801t CCC: $33.50
Published on Web 01/19/2006

have developed a nanoparticle "sandwich" assay in which two nanoparticle probes of different colors simultaneously recognize two binding sites on a single target molecule. This two-site sandwich method relies on a "double-selection" process to improve both detection sensitivity and specificity. Indeed, a number of powerful diagnostic technologies are based on this two-site sandwich format such as latex agglutination tests,[25] enzyme-linked immunoabsorbent assays (ELISA),[26] luminescent oxygen channeling immunoassay[27,28] (in which light emission arises from proximal diffusion of singlet oxygen species between two adjacent particles after target binding), and fluorescence cross-correlation spectroscopy.[29,30] In this format, target molecules do not need to be chemically derivatized, but the bound targets must be differentiated from excess probe.

Recent work has shown that dual-probe hybridization and two-color coincidence detection can differentiate single target molecules from free probes in homogeneous solution.[11,13,14] However, these studies were based on organic dyes and were limited by photobleaching, spectral overlapping, and technical difficulties in achieving "par-focality" for two or more excitation laser beams (overlapping of two or more probe volumes). To overcome these problems, luminescent quantum dots have been used for single-molecule detection in microfluidic channels,[31] but the previous work did not examine other nanoparticle probes and did not critically evaluate the efficiency and reproducibility of single-molecule detection. In a further advance, we have developed a two-color colocalization method for analyzing the arrival times of single photons on two simultaneous channels. In contrast to previous analysis of photoburst heights, this scheme analyzes single-photon events in real time as single target molecules flow through a capillary tube. A major finding is that energy-transfer nanoparticles (embedded with one or more donor/acceptor dye pairs for fluorescence resonance energy transfer) are superior probes for single-molecule counting because two or more colors can be excited with a single light source, similar to the case of semiconductor QDs. In addition, we have examined the key factors in two-color single-molecule detection, providing a framework for further improvements and applications.

We note that the concept of single-molecule detection by two-color fluorescence correlation is not new, but the use of quantum dots and energy-transfer nanoparticles will have major advantages in practical applications because of the significantly improved signal-to-noise ratios and the ability to excite different-colored nanoparticles with a single light source. Furthermore, in comparison with software-based systems that analyze single-molecule signals with a time lag, our hardware-based counting system as reported in this work allows real-time detection and discrimination at 1000 data points/s. This capability will be essential for flow sorting of two-color sandwiched molecules and nanostructures.

EXPERIMENTAL SECTION

Instrumentation. Single-molecule instrumentation was based on an inverted epifluorescence microscope, equipped with two photon-counting avalanche photodiodes (APD-1 and APD-2), a single-photon counting and coincidence analysis module attached to the microscope side port, and a capillary flow channel placed on the microscope stage. The photon counting and analysis module consisted of (i) one 100-μm pinhole (Melles Griot, Irvine, CA), (ii) high-performance band-pass optical filters, (iii) two aspheric focusing lenses (f = 11 mm, NA = 0.25, Thorlabs, Newton, NJ), (iv) two photon-counting detector, and (v) two XYZ translation stages (Newport Corp., Irvine, CA). A fused-silica capillary with diameters of 2.0 (inner) and 150.0 μm (outer) (Polymicro Technologies, Phoenix, AZ) was mounted onto an x−y mechanical stage of the microscope. A 1-cm window was cleared on the capillary for optical detection. The sample solution was injected into the capillary by a syringe. A continuous-wave argon ion laser (Lexel Laser, Fremont, CA) was used for excitation. The 488-nm line was reflected by a dichroic beam splitter (DC-1, 505 DRLP, Omega Optical Inc. Brattleboro, VT) and was focused into the capillary window through a high numerical aperture, oil immersion (n = 1.518) 100 ×/1.25 NA objective lens (Nikon Instrument Group, Melville, NY). Fluorescence light was collected through the same objective, passing through the dichroic beam splitter and the 100-μm pinhole, and was separated by another dichroic beam splitter (DC-2, 560 DCLP, Chroma Technology Corp., Brattleboro, VT). After a band-pass filter (BP-1/HQ514 M10 or BP-2/D670 M40, Chroma Technology Corp.), the green and red signals were separately focused on two avalanche photodiodes (SPCM-AQR-13, EG&G Canada, Vaudreuil, Canada) for single-photon detection.

Single-photon events were detected as voltage pulses with a width of ~50 ns and an amplitude of ~2.5 V. The APD-1 output was fed to a delay generator (Model 416a, Ortec, Oakridge, TN), which extended the pulse width to a controllable value in the range of 0.2−110 μs. The delay generator output and the ADP-2 output were fed into a universal coincidence unit (Model 418a, Ortec). The coincidence output was counted by using a multichannel scalar (EG&G Canada, Vaudreuil, Canada). At an integration time of 1 ms, this system permits high-speed detection of single molecules in a flow channel at 1000 data points/s.

Nanoparticle Bioconjugation. Oligonucleotides (oligos) or antibodies were covalently conjugated to nanoparticles by using standard conjugation chemistry.[32] For energy-transfer nanoparticles (40 nm) and quantum dots (3−5 nm), the number of oligo or antibody ligands per particle was approximately one (determined experimentally by using fluorescently labeled oligos or antibodies, as described in more detail below). These nearly "monovalent" nanoparticles produced excellent binding results

(24) Michalet, X.; Pinaud, F. F.; Bentolila, L. A.; Tsay, J. M.; Doose, S.; Li, J. J.; Sundaresan, G.; Wu, A. M.; Gambhir, S. S.; Weiss, S. *Science* **2005**, *307*, 538−544.

(25) Newman, D. J.; Henneberry, H.; Price, C. P. *Ann. Clin. Biochem.* **1992**, *29*, 22−42.

(26) Diamandis, E. P.; Christopoulos, T. K. *Immunoassay*; Academic Press: San Diego, 1996.

(27) Ullman, E. F.; Kirakossian, H.; Switchenko, A. C.; Ishkanian, J.; Ericson, M.; Wartchow, C. A.; Pirio, M.; Pease, J.; Irvin, B. R.; Singh, S.; Singh, R.; Patel, R.; Dafforn, A.; Davalian, D.; Skold, C.; Kurn, N.; Wagner, D. B. *Clin. Chem.* **1996**, *42*, 1518−1526.

(28) Ullman, E. F.; Kirakossian, H.; Singh, S.; Wu, Z. P.; Irvin, B. R.; Pease, J. S.; Switchenko, A. C.; Irvine, J. D.; Dafforn, A.; Skold, C. N.; Wagner, D. B. *Proc. Natl. Acad. Sci. U.S.A.* **1994**, *91*, 5426−5430.

(29) Schwille, P.; MeyerAlmes, F. J.; Rigler, R. *Biophys. J.* **1997**, *72*, 1878−1886.

(30) Rigler, R. *J. Biotechnol.* **1995**, *41*, 177−186.

(31) Stavis, S. M.; Edel, J. B.; Samiee, K. T.; Craighead, H. G. *Lab Chip* **2005**, *5*, 337−343.

(32) Hermanson, G. T. *Bioconjugate Techniques*; Academic Press: San Diego, 1996; pp 173−176.

while avoiding the problem of target/probe aggregation. Thus, a solution of green nanoparticles (40 nm, $\lambda_{ex} = 505$ nm, $\lambda_{em} = 515$ nm, 53 pmol) (Molecular Probes, Eugene, OR) was mixed with oligo-1 (5′-**CTTCAGTTTCTCGGG**-A_{10}-NH_2, 52.8 pmol) or oligo-2 (5′-NH_2-A_{10}-**CTCCTCCAGCTCCTT**-3′, 37.4 pmol) (Sigma Genosys, Woodlands, TX), together with an amine activation reagent (50 μg, sulfo-NHS, Pierce, Rockford, IL) in a pH 5.75 buffer (0.1 M morpholinoethanesulfonic acid). To this mixture was added a carbodiimide cross-linking agent (50 μg of 1-ethyl-3-(3-dimethylaminopropyl) carbodiimide (EDAC, Pierce), and the resultant mixture was thoroughly mixed and sonicated during a 2-h period at room temperature. Bioconjuagted nanoparticles were purified by centrifugation using S-400 Microspin columns (Amersham Bioscience, Piscataway, NJ) at 740*g*. Similar protocols were used to conjugate amine-modified oligos to other sized beads as well as semiconductor quantum dots. The bioconjugation efficiencies were determined by using fluorescently labeled amine-oligos (amine- A_{10}-CTCCTCCAGCTCCTT-Oregon Green; Sigma Genosys) and plain (nonfluorescent) 40-nm beads. After the cross-linking reaction, free unreacted oligos were separated from conjugated oligos by centrifugation. Fluorescence intensity measurements of the two fractions showed that ~11% of the oligos were conjugated to nanoparticles under our experimental conditions. The fraction of fluorescent beads obtained after passing through identical reaction scheme was also determined by fluorescence measurements before and after reaction. Finally, we used the stock concentrations of the probes and beads, and their known fractions retained during reaction and purification, to determine the number of conjugated ligands per nanoparticle. Our calculations indicated that there were ~1.2 ligand molecules/particle.

Similar protocols were used for antibody conjugation, such as monoclonal antibodies to rat anti-mouse/rat tumor necrosis factor-α (TNF-α; PharMingen/BD Biosciences, San Diego, CA). Antibody conjugated nanoparticles were blocked by using PBN buffer (0.5% bovine serum albumin (Sigma, St. Louis, MO) and 0.02% sodium azide in phosphate-buffered saline (PBS, Sigma)) and were purified by centrifugation with S-300 Microspin columns (Amersham Bioscience) at 740*g*. For respiratory syncytial virus (RSV) detection, two mouse monoclonal antibodies (clones 131−2G and 131−2A) (provided by Centers for Disease Control and Prevention, Atlanta, GA) were conjugated to green and red nanoparticles, respectively. The coupling and separation procedures were the same as described above.

Experimental Procedures. DNA hybridization was performed using 4× SSC−sodium dodecyl sulfate (1× SSC: 0.15 M sodium chloride and 0.015 M sodium citrate, pH 7.0) for 30 min at 45 °C. For cellular lysate studies, the original cell extract (9 mg/mL) was diluted 100 times. For control studies, several noncomplementary targets (total concentration, 3 pM) were added into the lysates. For specific binding studies, a complementary target (2 pM, 5′-CCCGAGAAACTGAAGAAGGAGCTGGAGGAG) was also added to the lysates. These samples were mixed with green probes (7.2 nM, 5′-CTTCAGTTTCTCGGG-A_{10}-3′-nano) and red probes (4.2 nM, nano-5′-A_{10}-CTCCTCCAGCTCCTT), followed by hybridization at 45 °C for 30 min.

Target protein TNF-α was determined by using sandwich immunoassay: 10 μL of green particles (2.8×10^{13} particles/mL) with the capture antibody was mixed with TNF-α (0.5 μL at 10 μg/mL, R&D System Inc., Minneapolis, MN) in 84.5 μL of PBN buffer. The mixture was incubated for 45 min at room temperature. To this mixture, a second biotinylated monoclonal antibody (3 μL at 25 μg/mL concentration) was added, followed by an incubation period of 30 min. Then, streptavidin-coated red nanoparticles ($\lambda_{ex} = 488$, $\lambda_{em} = 645$ nm, 40-nm diameter, 2 μL of 1.4×10^{14} particles/mL) (Molecular Probes) were added and allowed to incubate for 30 min. The final binding mixture was diluted 1000 times before single-molecule analysis.

Both mutated and wild-type RSV viruses were determined by using the following procedure: green probes coupled with purified mouse anti-G monoclonal antibody (clone 131−2G, 2.8×10^{13} particles/mL, 2 μL) and red nanoparticles coupled with purified mouse anti-F monoclonal antibody (clone 131−2A, 2.8×10^{13} particles/mL, 5 μL) were mixed with the viruses in 250 μL of PBS−TBN buffer (0.02% Tween 20, 0.1% bovine serum albumin, 0.02% azide). Binding of nanoparticle probes to virus surface proteins was allowed to proceed at 37 °C for 2 h. The mixture was then diluted 200 times before analysis.

For single-molecule analysis, samples were loaded into a capillary microchannel by microsyringe injection. The flow speed (0.55 mm/s) was determined and calibrated by measuring the time for the liquid to travel a known distance on the microscope stage.

Materials. Nuclear extract and lysates of Raji-B cells were kindly provided by Dr. Uma Nagarajan of Emory University. Except as noted, all chemicals and biochemicals were obtained from commercial sources. Poly(L-lysine hydrobromide) (MW = 350,000), Trizma base (tris(hydroxymethyl)aminomethane), trizma hydrochloride (tris(hydroxymethyl)aminomethane hydrochloride), 2-mercaptoethanol, coliphage T4 DNA, λ-DNA, T4 DNA ligase, histone protein, and bovine serum albumin were purchased from Sigma Chemical Co. Carboxylate-modified energy-transfer nanoparticles (40-nm diameter) (Fluosphere 505/515, product no. F-8795 and TransFluosphere 488/685, product no. T-8868) were purchased from Molecular Probes. Microscope coverslips (0.13 mm thick) were purchased from Fisher Scientific (Pittsburgh, PA). Ultrapure water was prepared by a Milli-Q purification system (Millipore, Bedford, MA).

RESULTS AND DISCUSSION

Detection Principles. The basic principles of single-molecule counting using nanoparticle probes are shown in Figure 1. In this scheme, two bioconjugated nanoparticles are designed to recognize the same target molecule at two different sites (antigenic sites or nucleic acid sequences). This sandwich-type binding brings two color-coded nanoparticles together to form a nanoparticle pair (Figure 1a). This pair moves in solution as a single complex and, when excited by a laser beam, emits green and red fluorescence light simultaneously (that is, spatial colocalization of two particles leads to time coincidence of their fluorescence signals). In contrast, unbound green and red particles move in a random fashion and are unlikely to pass through the laser beam at the same time (Figure 1b). Thus, coincident green and red light emission allows one to discriminate bound targets from excess unbound probes in a homogeneous solution mixture.

Both QDs and energy-transfer nanoparticles are well suited for single-molecule detection, and their unique optical properties

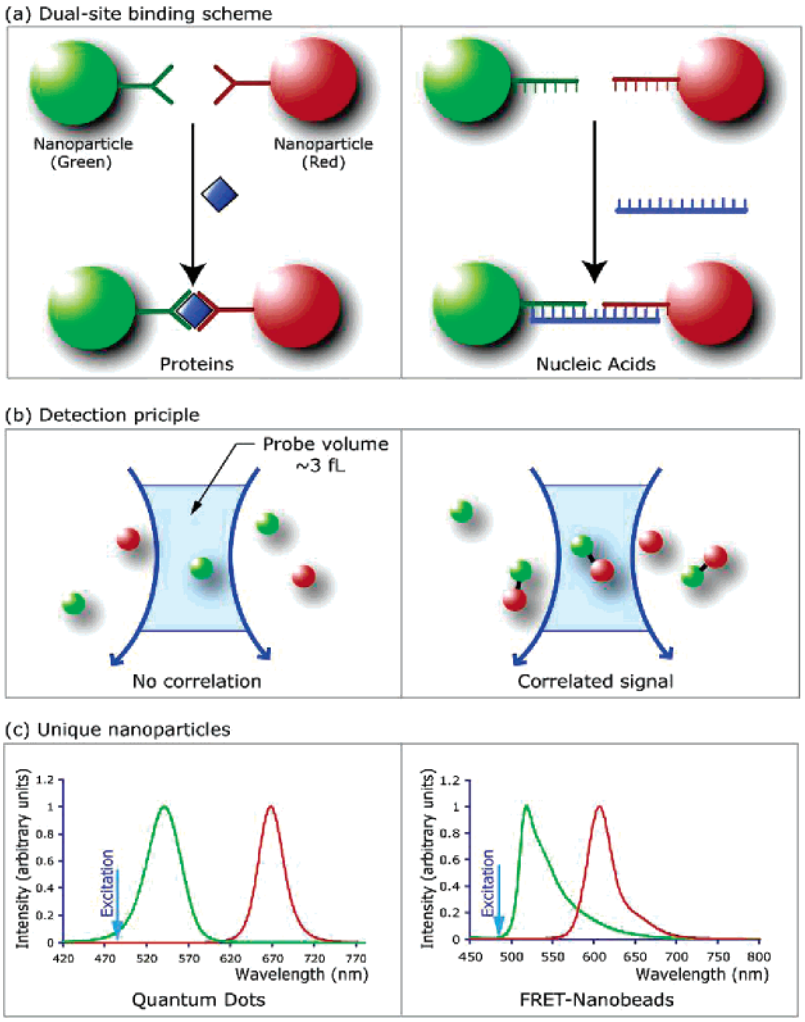

Figure 1. Schematic diagrams illustrating the principles of single-molecule sandwich assays using color-coded nanopartcles. (a) Simultaneous double-site binding for protein and nucleic acid detection; (b) free nanoparticle probes and bound sandwich pairs moving across a tightly focused laser beam; and (c) fluorescence emission spectra of color-coded quantum dots and energy-transfer nanoparticles. The left panel shows green and red QDs simultaneously excited with a single light source at 420 nm, and the right panel shows green and red energy-transfer nanoparticles excited at the same wavelength. The arrows indicate the relative position of the excitation laser wavelength (488 nm) used in single-molecule detection.

are shown in Figure 1c. A major advantage is that a single light source can be used to excite two or more fluorescence colors. A single excitation beam produces only one probe volume, and this overcomes the difficulties in focusing two color laser beams into a small confocal volume (femtoliter or 10^{-15} L). Weiss and co-workers[33] have shown that the cofocusing of two laser beams (par-focality) is an exceedingly difficult task due to both chromatic and spherical aberrations of the microscope objective. Klenerman and co-workers[13,14] reported that, even under carefully matched conditions, the volume overlap for two excitation laser beams was less than 30%. QDs and energy-transfer nanoparticles also have more symmetric and narrower emission spectra than single-color organic fluorophores, a feature that is important for minimizing spectral overlaps between two or more colors.

Single-molecule instrumentation is based on an inverted single-point confocal microscope, equipped with two photon-counting avalanche photodiodes (APD-1 and APD-2), a single-photon counting and coincidence analysis module (attached to the microscope side port), and a capillary flow channel placed on the microscope stage (Figure 2). In the photon analysis module, fluorescence light emitted from green and red nanoparticles is separated by a dichroic filter (DC-2) and is detected in real time by APD-1 and APD-2. The single-photon output signal from APD-1 is used to trigger a delay generator, which produces a voltage pulse with a controllable width. This modified pulse is fed into a coincidence event detector, and its preset width is used as a time window to determine whether one or more photons are detected by APD-2 during this time period. Using a standard photon-counting device such as a multichannel scalar, the coincidence output signals are recorded over a period of time. At an integration time of 1 ms, this system permits high-speed detection of single molecules in a flow channel at 1000 data points/s.

The logic and electronic hardware for real-time coincidence analysis of single photons is further shown in Figure 3. We discuss three representative cases for coincident photon detection on two APD detectors. Note that the system is activated by the detection of a single photon on APD-1, which generates a 50-ns-wide pulse of 2.5 V in amplitude and is converted to a new voltage pulse with

(33) Lacoste, T. D.; Michalet, X.; Pinaud, F.; Chemla, D. S.; Alivisatos, A. P.; Weiss, S. *Proc. Natl. Acad. Sci. U.S.A.* **2000**, *97*, 9461−9466.

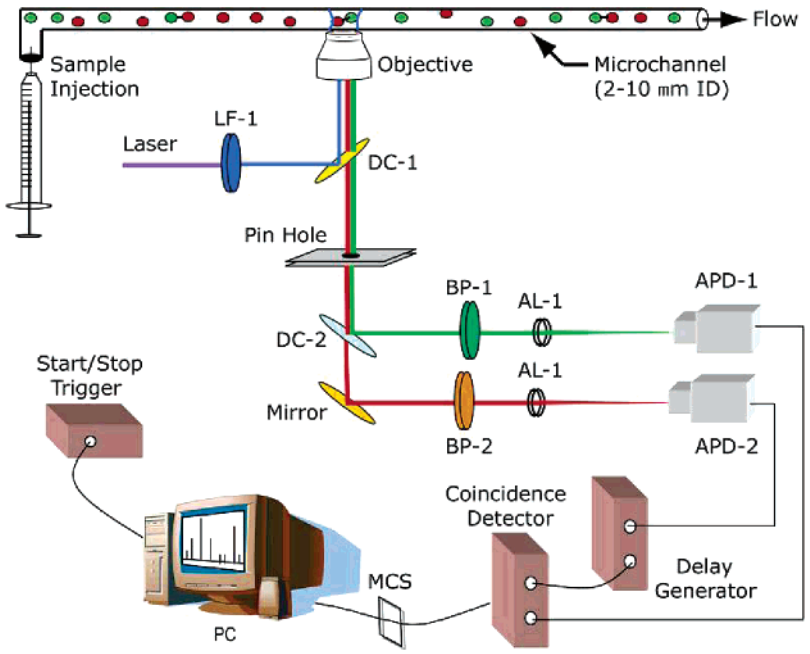

Figure 2. Instrumental diagram showing real-time detection of single nanoparticles and correlated sandwich pairs flowing in a small capillary. See text for detailed discussion. LF-1, laser filter; DC-1, dichroic filter in the microscope filter cube; DC-2, dichroic filter outside the microscope side port; BP-1, band-pass filter (HQ514 M10); BP-2, band-pass filter (D670 M40); AL-1 and AL-2, aspheric focusing lenses; ADP-1 and APD-2, single-photon counting avalanche photodiodes; MCS, multichannel scalar; PC, personal computer.

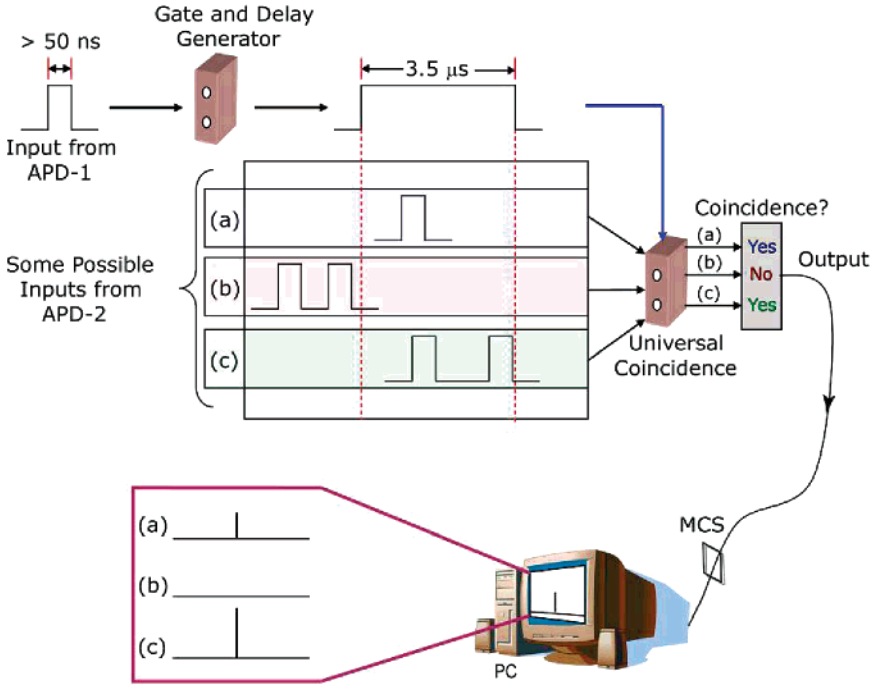

Figure 3. Logic and electronic hardware for real-time coincidence analysis of single photon events on two simultaneous detectors (ADP-1 and APD-2). See text for detailed discussion.

a controlled width (typically 3.5 μs; see below). In the first case (a), a single photon is detected by APD-2 during this 3.5-μs delay time, and the coincidence detector output is "1". In the second case (b), no photons are detected by APD-2 during this time window; the coincidence output is "0". In the third case (c), two separate photons are detected by APD-2; the coincidence output is "2". The coincidence output signals are recorded over a period of time at a bin or integration time of 1.0 ms for each data point. This allows real-time detection of single molecules based on the coincident arrival of green and red nanoparticle signals.

Single DNA Molecules. In addition to real-time recording of the coincidence signals, our "hard-wired" system permits simultaneous data recording from the individual APD channels. Figure 4 shows real-time photon burst data obtained from APD-1, APD-2, and the coincidence detector for DNA−nanoparticle bioconjugates in a capillary flow. For green-coded nanoparticles, intense single-particle signals are detected only on the green channel (APD-1), while for red-coded nanoparticles, intense signals are only detected on the red channel. For a sample of mixed green and red nanoparticles, both green and red signals

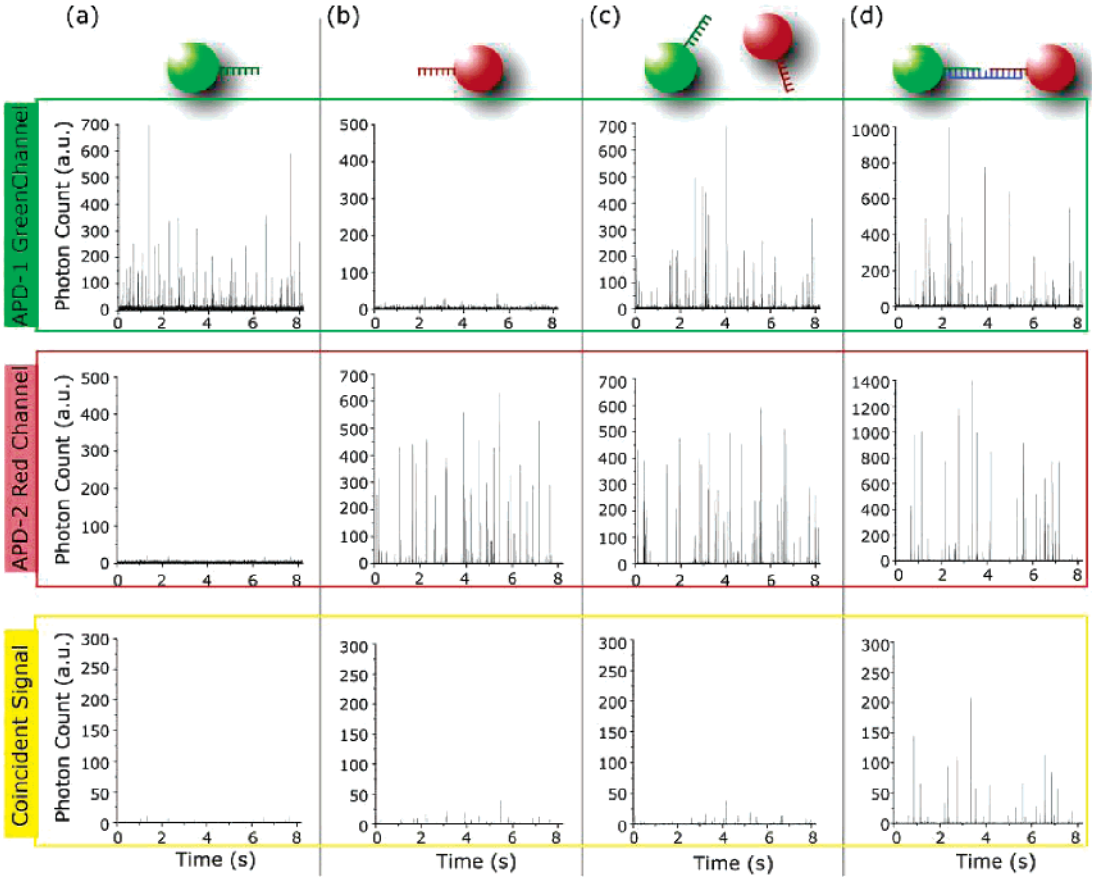

Figure 4. Real-time photon burst data obtained from DNA-conjugated nanoparticles in a microfluidic channel and simultaneously recorded from APD-1 (green channel), APD-2 (red channel), and the coincidence channel (yellow). (a) Green nanoparticle probes (5′-**CTTCAGTTTCTCGGG-**$(A)_{10}$-3′-nanoparticle, 7.2 pM); (b) red nanoparticle probes (nanoparticle-5′-$(A)_{10}$-CTCCTCCAGCTCCTT-3′, 4.2 pM): (c) a mixture of 7.2 pM green probes and 4.2 pM red probes (without a complementary DNA target); and (d) a mixture of 7.2 pM green probes and 4.2 pM red probes with a complementary DNA target (5′-**CCCGAGAAACTGAAG**-AAGGAGCTGGAGGAG-3′, 4.0 pM). Probe concentrations were determined experimentally after oligo conjugation and purification. Their values were controlled within a factor of 2 but were not identical because the differences in conjugation and purification efficiencies for each batch. Boldfaced and underlined letters denote complementary sequences. Microchannel inner diameter, 2.0 μm; liquid flow velocity, 0.55 mm/s; data acquisition speed, 1000 data points/s (integration time, 1 ms); delay time, 3.5 μs; laser wavelength, 488 nm; and laser intensity, 100.0 μW.

are observed, with only weak signals from the coincidence channel. Significantly, when a target DNA is used to hybridize to both probes, strong signals are detected on the coincidence channel.

It is worth noting that the coincidence signals are weak but still detectable from the data of individual green and red nanoparticles as well as their mixtures. For single-color particles, background coincidence signals arise from residual spectral overlaps between the green and red channels; that is, fluorescence signals in the red channel can "leak" into the green channel and vice versa. For the nanoparticle mixtures, background coincidence arises not only from spectral overlaping but also from random events in which a green particle and a red particle happen to pass the probe volume at the same time. Based on Poisson statistics, the probability of finding a red particle at 4 pM concentration in a 3-fL volume is ~0.72%, and that of a green particle at 7 pM in a 3-fL volume is 1.26% (the range of nanoparticle concentrations used in the experiment was 4−7 pM). The probability for finding a red particle and a green particle simultaneously in this volume is 0.009%, an exceedingly rare event that is unlikely to cause a major background problem.[34,35] Regardless the dominant source of false coincidence signals, the results in Figure 4 provide a threshold value (~50 counts/ms) for subtracting "false-positive" events from the true coincidence signals. As discussed below, the threshold values for false coincidence are dependent on the specific experimental conditions and can be determined for each nanoparticle system.

To investigate whether this counting method is able to discriminate against a large excess of unspecific DNA, the green and red nanoparticle probes were mixed with a nuclear extract of Raji-B cells, and coincidence signals were recorded with and without a complementary target (Figure 5a). The results reveal that coincidence signals are highly specific to complementary target DNA and are not affected by the complex environment of cell lysates (containing nucleic acids, proteins, lipids, and other biomolecules). Furthermore, we have investigated whether larger energy-transfer particles and smaller QDs could be used for two-color single-molecule detection. Based on the clear coincidence results in Figure 5b and c, we conclude that different sized particles in various formats can be used for counting single molecules and for discriminating excess unbound probes in homogeneous solution.

(34) Nie, S. M.; Chiu, D. T.; Zare, R. N. *Anal. Chem.* **1995**, *67*, 2849−2857.
(35) Nie, S.; Chiu, D. T.; Zare, R. N. *Science* **1994**, *266*, 1018−1021.

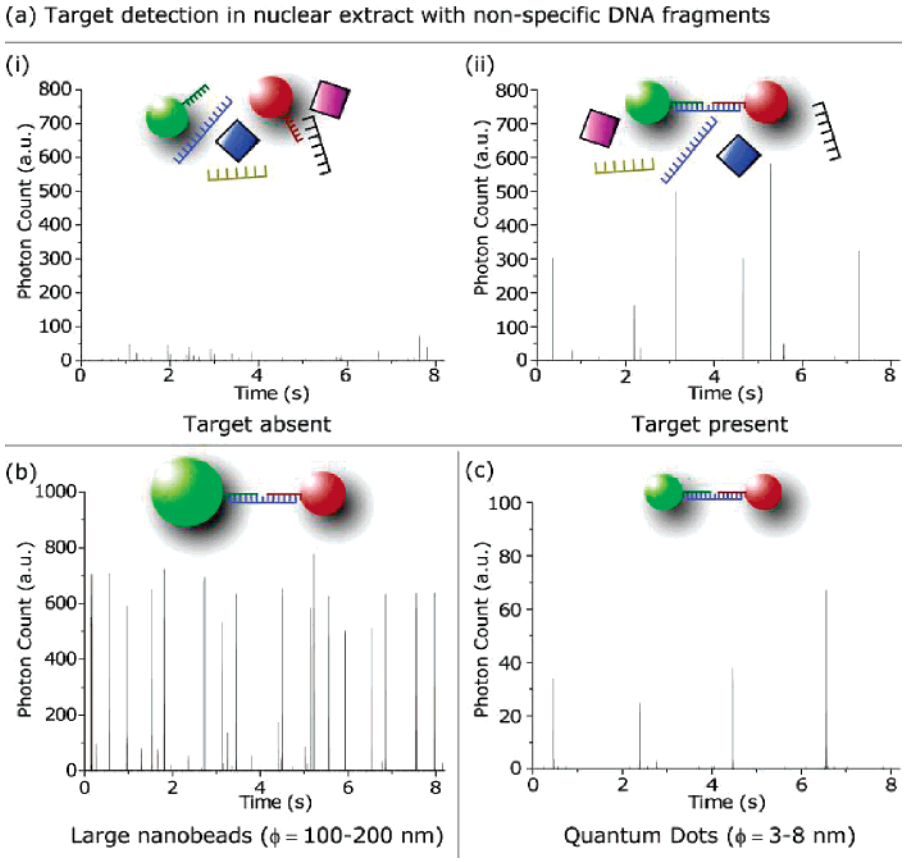

Figure 5. Single-molecule detection data obtained in (a) complex nuclear lysates, (b) using large energy-transfer particles of different sizes, and (c) using two-color semiconductor QDs. (a) Green and red nanoparticle probes mixed with Raji-B cell lysates with and without a complementary DNA target. The experimental conditions were the same as in Figure 4, except that the target DNA concentration was 2 pM. (b) Coincidence detection data using 200-nm green probes (4.5 pM) and 100-nm red probes (3.0 pM) in the presence of a complementary target (2 pM). (c) Coincidence detection data using 3.5-nm green QD probes (8 pM) and 5.5-nm red QD probes (7 pM) in the presence of a complementary target (4 pM).

In a systematic effort, we have examined several factors to optimize the performance of single-molecule counting. First, the optimal delay time is dependent on the photon emission rates of the nanoparticle probes and the specific experimental conditions. If this time window is too short, the coincidence detection clock will be reset before a photon is detected on APD-2, leading to a decrease or loss of coincidence signals. If this window is too long, even random photons would be detected as coincidence signals, leading to a high background. Under our experimental conditions (e.g., the rates of photon emission and 4−5% overall efficiencies for photon detection), statistical calculations suggest that the best signal-to-noise ratios are achieved with a delay time of 1−5 μs (R. Bailey and S. Nie, unpublished data). Experimental measurements of specific and nonspecific coincidence signals also indicate that the best results are obtained with a delay time of 3−4 μs. Thus, the delay time was set to 3.5 μs for most single-molecule detection studies.

Second, each nanoparticle should contain at least one ligand for target binding, but too many ligands per particle could lead to aggregation. This kind of aggregation causes an "undercounting" problem because multiple target molecules in a single aggregate will be counted as one molecule. This problem can be minimized by using "monovalent" probes (that is, each particle is conjugated to approximately one ligand). In this work, we prepared nearly monovalent probes (~1.2 ligands/particle) and worked at low probe and target concentrations. Third, in the absence of a hydrodynamic focusing mechanism, the nanoparticle probes are expected to follow random trajectories when moving across the laser beam, leading to path-dependent fluctuations in the signal intensity.[34,35] To correct for this problem, the excitation laser beam must completely fill or cover the capillary tube; that is, the laser beam cross section should be equal or larger than the channel cross section. However, our confocal laser beam is smaller than the 2-μm channel and can only detect ~70% of the passing particles, another source of errors leading to target undercounting. We note that the particle flow speed in 2-μm capillaries is ~0.55 mm/s (measured experimentally, see Experimental section). At this rate, it takes 0.5 ms for a particle to move across the laser beam waist (0.26 μm) and 4.3 ms to move through the defocused beam at a region near the channel wall. These transit times indicate that the integration times for each data point should be longer than 0.5 ms but shorter than 4.3 ms.

Single Protein Molecules. The above insights from DNA detection also apply to protein detection using two-color nanoparticle probes. Figure 6 shows real-time photon burst data obtained from two monoclonal antibody-conjugated nanoparticle probes with or without a protein target (50 pg/mL murine TNF-α factor, MW = 17 000). Similar to two-site DNA hybridization, the target protein simultaneously binds to two nanoparticle probes and generates colocalized fluorescence signals. Also, the control

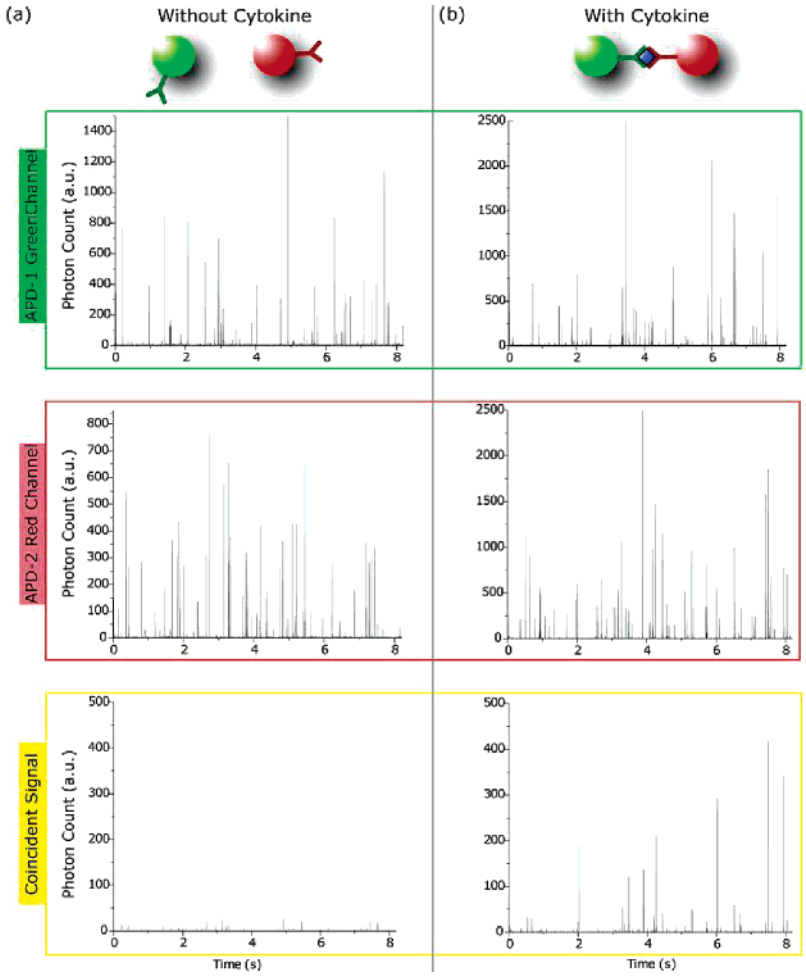

Figure 6. Real-time photon burst data obtained from antibody-conjugated nanoparticles in a microfluidic channel and recorded simultaneously from APD-1 (green channel), APD-2 (red channel), and the coincidence channel (yellow). (a) A mixture of green probes and red probes (4.7 pM each, conjugated to rat anti-monoclonal antibodies) in the absence of the target protein; (b) same as in (a) but with the target protein added (50 pg/mL recombinant murine TNF-α). The other experimental conditions were as in Figure 4.

data (without target protein) yield a threshold value for subtracting the background coincidence. A problem in protein detection, however, is that antibody−antigen interactions have finite dissociation equilibrium constants (k), on the order of 10^{-9}−10^{-12} M. Using second-order binding kinetics as a first approximation, an excess probe concentration equal to k leads to 50% target binding at equilibrium. To achieve 90% target binding, the excess probe concentration must be 9 times k. This simple analysis suggests that significant probe excess is needed to drive protein binding. On the other hand, excess probes will cause more background noise and, thus, interfere with single-molecule measurement. Based on the level of nonspecific background signals with cytokine antibodies, we estimate that the maximum probe concentrations might be increased to ~10−20 times of the equilibrium constant k to achieve 90−95% target binding.

An alternative approach is to mix the probes and targets at high concentrations and then dilute the mixture just before analysis. In this case, the stability of the complex becomes an important factor. Recent work by Klenerman et al.[14] has found that the dissociation rates for the IgG antibody−antigen complex are $\sim 3 \times 10^3$ s^{-1} and that the dissociation equilibrium constants for the antigen−antibody dimer Ag−Ab$_2$ are $\sim 2.3 \times 10^{-21}$ M^2. Under these conditions, quantitative measurement of protein−antibody complexes were reported over 3 orders of magnitude. The achieved sensitivity was limited by the slow rate for target molecules to encounter the probe laser beam by random diffusion. For example, at 50 fM concentration, the probability for a target molecule to diffuse into a 2-fL volume is only 0.006%;[34,35] that is, a target molecule will stay in the laser beam for only 1 ms in a data acquisition period of 15−20 s. To increase the probability of target/laser encounters, the laser beam can be rapidly scanned across the sample (target search), or a microfluidic device can be used to rapidly flow the sample through the laser beam. In the current work, we have used the flow approach to increase the number of counted target molecules per unit time. It is worth noting that the total sample volumes to be consumed with micrometer-sized channels are only a few nanoliters for the entire single-molecule counting measurement. This ability is very important to single-molecule studies in small-volume samples such as single cells but will become a problem in analyzing or screening large-volume samples.

Single Intact Viruses. By using proper and specific antibodies, bioconjugated nanoparticles also allow rapid and sensitive detection of single intact viruses. For example, we have detected single RSV particles in a homogeneous sample. This virus causes serious lower respiratory tract illness in infants and young children

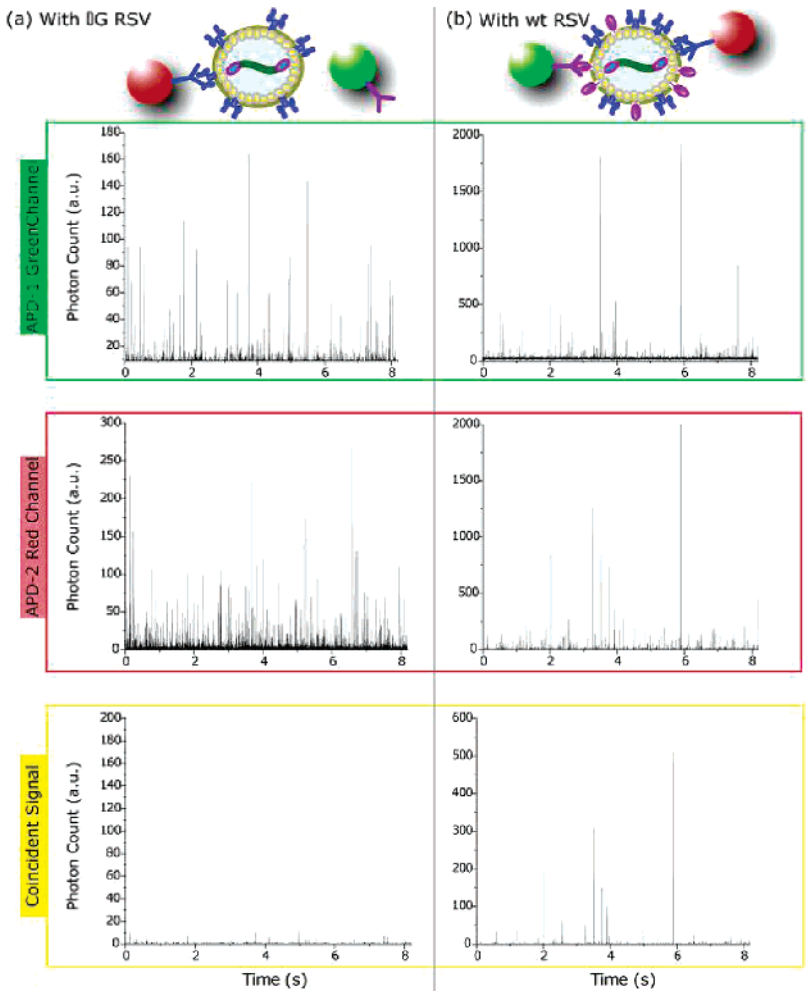

Figure 7. Real-time photon burst data obtained from antibody-conjugated nanoparticles mixed with intact RSV viruses and recorded simultaneously from APD-1 (green channel), APD-2 (red channel), and the coincidence channel (yellow). (a) Mutated virus RSV ΔG (with the G protein deleted) and (b) wild-type RSV with both F and G proteins expressed on the virus surface. RSV (4×10^6 pfu) was allowed to bind to two monoclonal antibodies against the G-attachment protein epitope (clone 131−2G) and the F-fusion protein epitope (clone 131−2A), respectively. The F-protein antibody was conjugated to red nanoparticles, and the G-protein antibody was conjugated to green nanoparticles. A 9-μm capillary channel was used to prevent clogging, and the other experimental conditions were the same as in Figure 4.

and is a significant pathogen of the elderly and immune compromised.[36,37] Rapid and sensitive RSV diagnosis is vital to controlling nosocomial infections and for ambulatory and long-term care patients, but current methods are limited by assay sensitivity and slow response. Figure 7 shows photon-coincidence results obtained from the wild-type RVS (with both F and G proteins expressed on the virus surface) and a mutated virus RSV ΔG (with the G protein deleted).[38,39] Intense coincidence signals are detected from the wild-type viruses because both green and red probes bind to the F and G viral proteins, respectively. The signals on all three channels are abnormally high, because a single virus has many copies of F and G proteins and is thus able to bind to many green and red particles. In comparison, the mutated virus gives little or no coincidence signal because the G protein is not available for binding to green particles. It is worth noting that the photon burst intensities on the red channel (F protein) are considerably lower than that of the wild-type virus, suggesting that the level of F protein expression is much lower on the mutated virus than on the wild-type virus.[40]

Detection Limit and Quantification. To evaluate the detection limit and other quantitative aspects of this nanoparticle counting technology, we carried out target DNA concentration studies over 6 orders of magnitude (fM−nM) while keeping the probe concentrations constant. At each target concentration, the number of counted targets was recorded in a period of 80 s and was repeated 10 times. This gives an average count and a standard deviation for each concentration. Figure 8 depicts the single-molecule counts as a function of target concentration. The small error bars indicate quantitative and reproducible counting of single molecules, except when the total number of counts falls below 10 (due to statistical or shot noise). Since both the target concentration and the sample flow rate are known, we calculate the actual number of target molecules that flow through the capillary in an 80-s period (dotted line). A comparison with the

(36) Couch, R. B.; Englund, J. A.; Whimbey, E. *Am. J. Med.* **1997**, *102*, 2−9.
(37) Falsey, A. R.; Walsh, E. E. *Clin. Microbiol. Rev.* **2000**, *13*, 371−384.
(38) Tripp, R. A.; Moore, D.; Jones, L.; Sullender, W.; Winter, J.; Anderson, L. J. *J. Virol.* **1999**, *73*, 7099−7107.
(39) Wertz, G. W.; Moudy, R. M. *Pediatr. Infect. Dis. J.* **2004**, *23*, S19−24.
(40) Agrawal, A.; Tripp, R. A.; Anderson, L. J.; Nie, S. *J. Virol.* **2005**, *79*, 8625−8628.

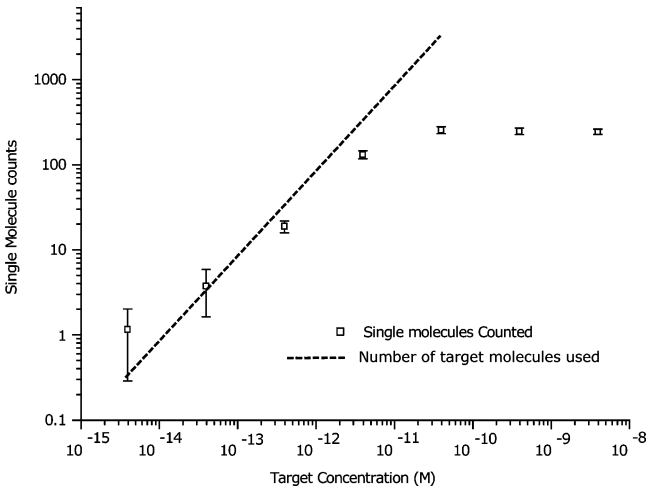

Figure 8. Single-molecule counting efficiencies and standard errors at different target DNA concentrations. The data points (squares) are actual target counts at various DNA concentrations, while the dotted line shows the theoretical numbers of target molecules passing through the probe volume. The counting data are the mean values ± standard error (n = 10). Note the "flat" region at high target concentrations, similar to the "hook effect" in ELISA and other sandwich-type immunoassay. See text for detailed discussion.

experimental data indicates that ~40% of the molecules are detected, below the 70% value derived from the expected cross-sectional area overlap between the laser beam and the capillary tube. As noted earlier, this discrepancy is likely caused by incomplete targeting binding and target−nanoparticle aggregation. Further improvements can be made by optimizing the excitation beam profile as well as the target binding/aggregation conditions.[41]

An interesting feature is that the number of detected molecules reaches a peak and then slowly decreases with increasing target concentration. This decrease is similar to the "hook effect" in sandwich-type immunoassays,[26] because excess targets cannot generate more sandwich pairs but can cause a breakup of double-binding pairs (Ab_1−Ag−Ab_2) to single-binding complexes (Ab_1−Ag and Ag−Ab_2). The single-binding complexes only show single-color signals and are not detected by the coincidence detector. At the low-concentration end, the detection sensitivity is determined by statistical noise, that is, the number of molecules that could be counted in a reasonable period of time. With a data acquisition time of 80 s and 2-μm flow channels, our data indicate that single molecules can be detected from target concentrations as low as 20−30 fM.

A major advantage of single-molecule detection is that target molecules do not need to be amplified for analysis. In current techniques using biochips and polymerase chain reactions (PCR), small samples are not analyzed directly but are amplified to create a final product for measurement. The amplification process can increase the target material as much as 1 million-fold, but it also can introduce errors and uncertainties. Unlike the relative gene or protein expression information obtained from microarrays, single-molecule counting can provide a way to make absolute measurements, which are required for clinical analysis of biomolecular markers in disease detection and diagnosis.[42] For this application, it is important to note that our nanoparticle counting technology does not require color-coded nanoparticles to couple or interact with each other; it only requires them to spatially colocalize or correlate within the optical diffraction limit of $\lambda/2$ (half of the wavelength or ~250 nm). It is thus broadly applicable to genes, proteins, and viruses. In addition, multiplexed single-molecule counting will be possible with the use of spectrally encoded nanoparticles,[43] which should allow a panel of 5−10 biomolecular markers to be analyzed in body fluid samples (e.g., blood serum). In comparison, other signal amplification methods using nanoparticle bio bar codes and surface plasmon resonance nanosensors do not automatically operate in the single-molecule detection or "digital" mode.[44,45]

In conclusion, we have developed a single-molecule counting method based on the use of nanoparticle probes and two-color fluorescence coincident detection. The results demonstrate real-time detection of single genes, proteins, and intact viruses in a microfluidic flow channel. The target molecules do not need to be derivatized chemically with a fluorophore and do not need to be amplified with PCR or other means. The achieved single-molecule counting is a "single-tube, homogeneous assay" because complex mixures can be analyzed without washing or a separation step. In addition, semiconductor QDs and energy-transfer nanoparticles are both bright and stable nanoprobes that are well suited for simultaneous excitation with a single light source. We envision that this molecular counting technology will have broad applications in ultrasensitive medical diagnostics, infectious agent detection, and intracellular single-molecule imaging, in which excess probes cannot be separated or washed away.

ACKNOWLEDGMENT

We thank Dr. William Doering for helpful discussions, Dr. Uma Nagarajan for providing Raji-B cell lysates, and Dr. Robert Bailey for help on water-soluble quantum dots. The work was supported in part by NIH grants (P20 GM072069, R01 CA108468-01 R01 GM60562, and U01 HL080711), the DOE Genomes to Life Program, and the Georgia Cancer Coalition Distinguished Cancer Scholars Program (to S.N.).

(41) Roos, P.; Skinner, C. D. *Analyst* **2003**, *128*, 527−531.
(42) Liotta, L.; Petricoin, E. *Nat. Rev. Genet.* **2000**, *1*, 48−56.
(43) Han, M.; Gao, X.; Su, J. Z.; Nie, S. *Nat. Biotechnol.* **2001**, *19*, 631−635.
(44) Nam, J. M.; Thaxton, C. S.; Mirkin, C. A. *Science* **2003**, *301*, 1884−1886.
(45) Haes, A. J.; Chang, L.; Klein, W. L.; Van Duyne, R. P. *J. Am. Chem. Soc.* **2005**, *127*, 2264−2271.

Received for review October 7, 2005. Accepted December 13, 2005.

AC051801T